

---

# *Contents*

<b>1</b>	<b>Efficient Multi-Material Topology Optimization</b>	<b>3</b>
	<i>Amir M. Mirzendehtel and Krishnan Suresh</i>	
1.1	Introduction . . . . .	3
1.2	Literature Review . . . . .	4
1.3	Proposed Method . . . . .	7
1.4	Numerical Experiments . . . . .	13
1.5	Contributions . . . . .	17
1.6	Acknowledgements . . . . .	18



# 1

---

## *Efficient Multi-Material Topology Optimization*

**Amir M. Mirzendehtel**

Research Scientist, Palo Alto Research Center, Palo Alto, CA

**Krishnan Suresh**

Professor, University of Wisconsin-Madison, Madison, WI

1.1	Introduction .....	3
1.2	Literature Review .....	3
1.3	Proposed Method .....	6
1.4	Numerical Experiments .....	13
1.5	Contributions .....	16
1.6	Acknowledgements .....	18
	References .....	19

---

### **1.1 Introduction**

This chapter focuses on generating optimized topologies using multiple materials. The interest in multi-material topology optimization (MMTO) stems from the well-recognized synergy between topology optimization (TO) and additive manufacturing (AM), where organic structures created through TO can be directly fabricated by a variety of AM processes. Given the rapidly increasing capabilities of AM, there is an opportunity to improve the performance of consumer products, biomedical, and aerospace components, through simultaneous optimization of topology and distribution of multiple materials.

Researchers have proposed various MMTO strategies [24, 11] to address this need (please see literature review in Section 2). However, these strategies are computationally intensive, and not well-suited for complex 3D design problems. An additional limitation is that they require the desired volume fraction for each material to be specified. This imposes an unnecessary burden on the designer. In the present chapter, we address both deficiencies by proposing a MMTO framework that is not only efficient, but it also eliminates the need to specify *a priori*, the desired material composition. The proposed framework is based on tracing Pareto frontiers, and is a generalization of the single-material Pareto method proposed in [16]. Through this generalization, a series of multi-material optimized solutions are generated. Furthermore, we show that the method can be easily ported to the cloud, providing easy access to designers from around the world. Figure 1.1 illustrates the proposed cloud based MMTO and AM framework.

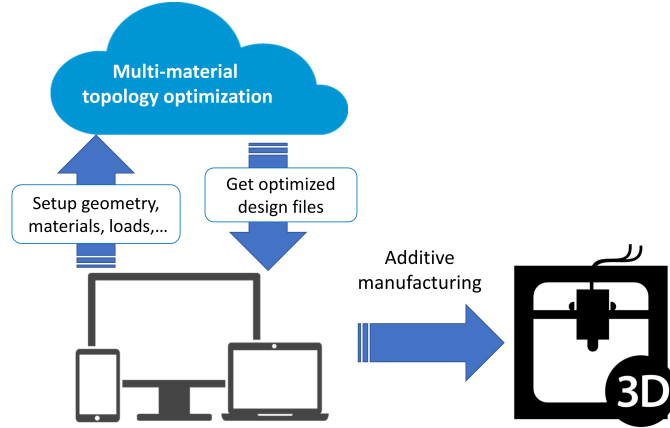


FIGURE 1.1: Overview of the proposed MMTO framework.

## 1.2 Literature Review

In multi-material topology optimization (MMTO), one must simultaneously optimize the topology, and the distribution of various materials within the topology. A typical MMTO compliance minimization problem can be posed as:

$$\begin{aligned}
 & \underset{\Omega_{k=1,\dots,M} \subset D}{\text{minimize}} && J(\Omega, \mathbf{u}) = \mathbf{f}^T \mathbf{u} \\
 & \Omega_i \cap \Omega_{i \neq j} = \emptyset && i, j = 1, \dots, M \\
 & g_n(\Omega, \mathbf{u}) \leq 0 && n = 1, \dots, N \\
 & \text{subject to} && \\
 & \mathbf{K}\mathbf{u} = \mathbf{f} && 
 \end{aligned} \tag{1.1}$$

where  $J$  is compliance,  $M$  is the number of materials, and  $\Omega_k$  is the topology for  $k^{\text{th}}$  material to be computed. Thus, the objective is to find the optimal distribution of  $M$  non-overlapping materials, within a given design space, that minimizes a specific objective and satisfies certain design constraints. The MMTO problem posed in Equation 1.1 assumes that every point within the design space has a distinct material associated with it (or is void). This differs from functionally graded material optimization, where a mixture of base materials is allowed.

Below, we briefly review various strategies that have been proposed to solve such MMTO problems.

### 1.2.1 SIMP-Based MMTO

The classic Solid Isotropic Material with Penalization (SIMP) strategy for topology optimization, was first extended to multiple materials in 1992 [19]. A unique and challenging aspect of SIMP is that one must carefully assign interpolation schemes for different material properties. These are discussed in [14], where Sigmund proposed a two-material interpolation scheme for designing thermally, and electrothermally driven micro-actuators. An alternate material interpolation strategy was developed in [25] by introducing a peak function and exploiting optimality criteria method.

A new SIMP method was presented in [7] for optimizing multiple homogeneous materials, which interpolates the stiffness matrix instead of interpolating the Young's modulus. The validity of this

method was demonstrated through 2D examples involving two materials. In [3], Chavez and Cunha implemented SIMP to solve a specific problem of minimizing the compliance of concrete slabs reinforced with carbon fibers. Their approach relies on concrete failure criteria, and the fact that the slabs are simple symmetric geometries in 2D. In 2007, De Kruijf et al. employed SIMP to minimize both compliance and resistance to heat dissipation of composites; the method was limited to 2D, and attains only the upper limits of Hashin-Shtrikman [4]. If the materials are composites, it is well-known that SIMP interpolations can violate Hashin-Shtrikman bounds [15]. Blasques and Stolpe proposed a density based framework for minimizing compliance of laminated composite beam cross sections [2]. The method allows multimaterial laminates in 2D, where the formulation is carried out by writing equilibrium between laminate layers, under the limiting assumptions that the beam is slender and has invariant cross sections. A new multi-resolution scheme for MMTO was developed in [11], where different levels of discretization were employed for representing displacement, design variables, and density. The method uses the alternating active phase algorithm, in which the original problem is decomposed into a number of sub-problems, where only two of the materials are active, and is solved using the density approach.

### 1.2.2 Level-Set MMTO

In 2003, Wang and Wang extended the level-set based topology optimization to address multiple materials [22]. The method requires  $M$  level sets to represent  $2M$  distinct materials, and the proposed strategy was used to solve benchmark problems in 2D, where different colored level sets represented distinct materials. Later, the idea was expanded toward compliant mechanism design [21] and microstructures [23]. Unfortunately, as demonstrated in [1], the underlying shape derivatives were approximations, and relied on certain assumptions. Allaire and coworkers developed the correct mathematical shape derivatives in [1], where the interface zone thickness is also kept constant. In order to remove discontinuity caused by sharp interfaces, Vermaak et al. [20] suggested using multiple intermediate interfaces to attain continuity. The challenges in level-set based MMTO are: (1) field discontinuity, and (2) thickness diffusion. The former is due to the discontinuity in phase properties, which leads to discontinuous normal strain and tangential stress. The latter is caused by numerical diffusion in the level-set process [1].

### 1.2.3 Element Sensitivity Methods for MMTO

In 2010, Ramani developed an algorithm, based on the concept of *pseudo element sensitivity*, for compliance minimization of MMTO problems [12]. The algorithm starts with computing and ranking element sensitivities, where for each element, two sensitivities are computed: the first sensitivity is the expected change in objective when the element material is changed to the next heavier material, and the second sensitivity is the expected change in objective when the element material is changed to the next lighter material. Then, the material distribution undergoes a repeated cycle between feasible and infeasible solutions, until it converges. Ramani extended this in 2011 to stress-constrained MMTO [13].

The work presented in this chapter uses the concept of element sensitivity; however:

1. The connection between element sensitivity and well-known topological sensitivity is illustrated. Thus, the concept of element sensitivity can be generalized to arbitrary quantities of interest.
2. In [13], the intermediate designs may be structurally disconnected. Therefore, as the author states, it is critical that void elements be assigned a low value of Young's modulus. In the present work, since every intermediate is Pareto-optimal, it is necessarily connected, and

therefore, void elements can be suppressed without resulting in singularity. This leads to better condition number and faster convergence.

3. Displacement constraints are handled in [12] by switching between “infeasible” and “feasible” designs. Here, all intermediate designs satisfy the displacement constraint, and the designer has the option of choosing from a multitude of Pareto-optimal designs.
4. The material changes in [13] are restricted by the two sensitivities described above, this may lead to suboptimal designs. Here, this limitation is eliminated, and is illustrated later through numerical experiments.

### 1.2.4 Nomenclature

For clarity and reference, we summarize below the symbols used in this chapter.

$\Omega$	Overall topology
$\Omega_i$	Topology for $i^{\text{th}}$ material
$D$	Design domain
$ \Omega $	Volume of overall topology
$ \Omega_i $	Volume of topology for $i^{\text{th}}$ material
$V^*$	Allowed total volume
$V_i^*$	Allowed total volume for material $i$
$\rho_i$	Density of material $i$
$\mathcal{M}$	Allowed total mass
$J$	Compliance
$\mathbf{K}$	Stiffness matrix
$\mathbf{u}$	Displacement vector
$\mathbf{f}$	External force vector
$g$	Generic constraint
$\sigma$	Stress tensor
$\varepsilon$	Strain tensor
$\nu$	Poisson's ratio
$\mathcal{T}_J(p)$	Topological sensitivity of compliance at point $p$
$\lambda$	Lame's first parameter
$\mu$	Lame's second parameter
$\phi$	Quantity of interest
$D_\phi(e)$	Discrete sensitivity of quantity of interest at finite element $e$
$D_J(e)$	Discrete sensitivity of compliance at finite element $e$
$\mathbf{K}_e$	Stiffness matrix of element $e$
$\mathbf{u}_e$	Displacement vector of element $e$
$\Delta J_e^{k \rightarrow m}$	First order element sensitivity for compliance of swapping material $k$ with $m$ at element $e$
$\Delta J_e^{k \rightarrow \emptyset}$	First order element sensitivity for compliance of removing element $e$ with material $k$
$\Delta J_e^{\emptyset \rightarrow k}$	First order element sensitivity for compliance of adding element $e$ with material $k$
$\Delta M_e^{\emptyset \rightarrow k}$	Change of mass for swapping material $k$ with $m$ at element $e$
$\theta_e^{k \rightarrow m}$	Ratio of element sensitivity over change in mass for swapping material $k$ with $m$ at element $e$
$r^1(e)$	Ranking parameter at element $e$ for reducing mass sub-step
$r^2(e)$	Ranking parameter at element $e$ for reducing compliance sub-step

### 1.3 Proposed Method

Since the proposed method generalizes the topological sensitivity based single-material Pareto-tracing method [16, 9] to multiple materials, we briefly summarize the concept of topological sensitivity, its relationship to element sensitivity, and the single-material Pareto method.

#### 1.3.1 Topological vs. Element Sensitivity

Topological sensitivity is defined as the first order change in a quantity of interest, when an infinitesimal hole is inserted in a domain. A closed-form expression for the topological sensitivity for compliance in 2D homogeneous isotropic materials is given by [5]:

$$\mathcal{T}_J(p) \equiv \frac{4}{1+\nu} \boldsymbol{\sigma} : \boldsymbol{\varepsilon} - \frac{1-3\nu}{1-\nu} \text{tr}(\boldsymbol{\sigma}) \text{tr}(\boldsymbol{\varepsilon}) \quad (1.2)$$

This has also been generalized to 3D [10]:

$$\mathcal{T}_J(p) \equiv -20\mu \boldsymbol{\sigma} : \boldsymbol{\varepsilon} - (3\lambda - 2\mu) \text{tr}(\boldsymbol{\sigma}) \text{tr}(\boldsymbol{\varepsilon}) \quad (1.3)$$

where  $\lambda$  and  $\mu$  are the Lamé' parameters. Similar topological sensitivity fields can be computed for various performance metrics, both in 2D and 3D [16].

Observe that the topological sensitivity can be computed as a post-processing step after a finite element analysis is carried out. An intuitive interpretation of topological sensitivity is that regions of low sensitivity correspond to regions with relatively low impact on performance, and can therefore be targeted for removal. For other quantities of interest such as anisotropic strength, and for multi-material scenarios, no closed-form expressions for topological sensitivity exist. We will therefore consider an alternate *discrete element sensitivity*, defined, for each element, as the change in any quantity of interest when a single element  $e$  is deleted from the mesh:

$$\mathcal{D}_\varphi(e) \equiv \frac{\varphi(\Omega - e) - \varphi(\Omega)}{|e|} \quad (1.4)$$

where  $|e|$  is volume of a single finite element, and is assumed to be negligible with respect to the volume of topology ( $|e| \ll |\Omega|$ ). It is easy to show that the element sensitivity for compliance is given by [8]:

$$\mathcal{D}_J = \mathbf{u}_e^T \mathbf{K}_e \mathbf{u}_e \quad (1.5)$$

As the element size shrinks to zero, one can expect the element sensitivity to approach the topological sensitivity. Indeed, Figure 1.2 compares topological sensitivity and element sensitivity for compliance for the 2D L-bracket. Observe that the two fields are quite similar since they essentially capture the first order change in compliance when material is removed. However, element sensitivity is easy to compute for arbitrary quantities of interest.

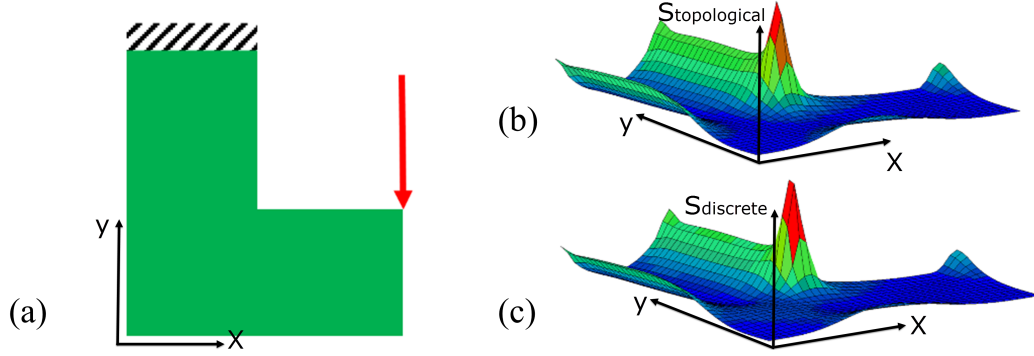


FIGURE 1.2: (a) L-bracket geometry, (b) topological sensitivity and (c) discrete element sensitivity.

### 1.3.2 Volume vs. Mass Formulations

A common method for solving the MMTO problem in Equation 1.1 is to impose a desired volume constraint on each of the constituent material [23]:

$$\begin{aligned}
 & \underset{\Omega_{k=1,\dots,M} \subset D}{\text{minimize}} && J(\Omega, \mathbf{u}) = \mathbf{f}^T \mathbf{u} \\
 & && |\Omega| \leq V^* \\
 & && |\Omega_k| \leq V_k^* \\
 & && \Omega_i \cap \Omega_{i \neq j} = \emptyset && i, j = 1, \dots, M \\
 & && g_n(\Omega, \mathbf{u}) \leq 0 && n = 1, \dots, N \\
 & && \text{subject to} \\
 & && \mathbf{K}\mathbf{u} = \mathbf{f}
 \end{aligned} \tag{1.6}$$

where  $J$  is compliance,  $|\Omega|$  is the total volume,  $|\Omega_k|$  is volume of  $k^{\text{th}}$  material. Unfortunately, these constraints reduce the design space, and also impose an additional burden on the designer since the designer must guess, *a priori*, the upper limit for the constituent materials.

Consider now an alternate total-mass-constrained formulation:

$$\begin{aligned}
 & \underset{\Omega_{k=1,\dots,M} \subset D}{\text{minimize}} && J(\Omega, \mathbf{u}) = \mathbf{f}^T \mathbf{u} \\
 & && \sum_{k=1,\dots,M} \rho_k V_k \leq \bar{\mathcal{M}} \\
 & && \Omega_i \cap \Omega_{i \neq j} = \emptyset && i, j = 1, \dots, M \\
 & && g_n(\Omega, \mathbf{u}) \leq 0 && n = 1, \dots, N \\
 & && \text{subject to} \\
 & && \mathbf{K}\mathbf{u} = \mathbf{f}
 \end{aligned} \tag{1.7}$$

Observe that the constraint is on the total mass of the design. In other words, no additional constraint is imposed on the relative volume fraction of each material. In the absence of such constraints, we are more likely to converge to better-performing designs; this was confirmed in [6].

Taking this one step further, the constraint on the total-mass can also be eliminated by considering

a two-objective generalization of Equation 1.7:

$$\begin{aligned}
 & \underset{\Omega_{k=1,\dots,M} \subset D}{\text{minimize}} \{J, \mathcal{M}\} \\
 & \sum_{k=1,\dots,M} \rho_k V_k = \mathcal{M} \\
 & \Omega_i \cap \Omega_{i \neq j} = \emptyset \quad i, j = 1, \dots, M \\
 & \text{subject to} \\
 & \mathbf{K}\mathbf{u} = \mathbf{f}
 \end{aligned} \tag{1.8}$$

This would allow us generate multiple Pareto-optimal solutions, rather than a single solution at the desired total-mass.

### 1.3.3 Single material Pareto Method

With this background, consider the Pareto method proposed in [16] for solving the single-material bi-objective TO problem:

$$\begin{aligned}
 & \underset{\Omega \subset D}{\text{minimize}} \{J, \mathcal{V}\} \\
 & \text{subject to} \\
 & \mathbf{K}\mathbf{u} = \mathbf{f}
 \end{aligned} \tag{1.9}$$

To solve the above problem, in the Pareto-method, one starts with the full design-space, i.e., design of volume fraction 1.0. Then, the target volume fraction is decremented by a small amount (with an initial decrement of 0.05, that is dynamically updated). The Pareto-optimal design, for that volume fraction, is computed using topological sensitivity, and a fixed-point iteration, as described in[16]. Typically, three to four FEA operations are needed for generating a Pareto-optimal design. Once this is complete, the target volume fraction is decremented gradually, resulting in a series of Pareto-optimal designs as illustrated in Figure 1.3. The optimization stops when a constraint is violated, and additional Pareto-optimal designs cannot be generated.

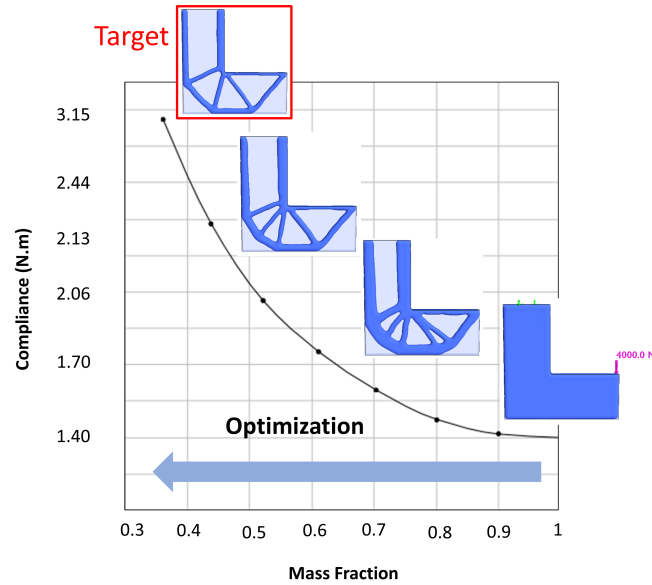


FIGURE 1.3: Single-material Pareto tracing.

Pareto differs from classic SIMP based methods in three ways: (1) in Pareto-method, a constraint on the final desired volume fraction is not needed since all Pareto-optimal designs that satisfy other performance constraints are generated, (2) Pareto-method relies on topological sensitivity rather than on pseudo-densities, and (3) since the intermediate designs are Pareto-optimal, the stiffness matrices are inherently better conditioned, leading to faster convergence of iterative solvers.

### 1.3.4 Multi-material Pareto Method

In the same spirit, the multi-material Pareto method, proposed here, generates a series of Pareto-optimal multi-material designs that satisfy the imposed constraints. The proposed algorithm starts with the heaviest design. Then, instead of decreasing the volume fraction, the mass fraction is decreased gradually, and Pareto-optimal multi-material designs are generated at each step. Further, instead of relying on topological sensitivity, we rely on discrete (element) sensitivity since closed-form expressions for multi-material topological sensitivity do not exist.

To ensure that that the Pareto curve is traced, each step consists of two sub-steps: (1) the total mass is reduced by a small decrement (sub-algorithm 1), followed by (2) a reduction in compliance (sub-algorithm 2). These two sub-steps are repeated until the next Pareto-optimal design is reached; see Figure 1.4. Then, the entire process is repeated to generate the entire Pareto curve, and associated multi-material designs.

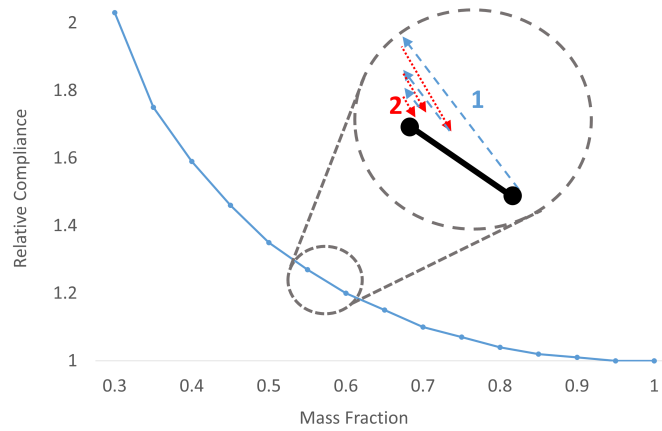


FIGURE 1.4: Tracing Pareto curve, and the two sub-steps.

Both sub-steps rely on a common theme of 'swapping' materials associated with elements. Observe that, at any instance, each element is associated with some material  $k$  (the material can also be void). Now consider a hypothetical swapping of the material  $k$  with material  $m$ . Observe that the change in compliance is given by the first-order element sensitivity (see Equation 1.5):

$$\Delta J_e^{k \rightarrow m} = \mathbf{u}_e^T \mathbf{K}_e^k \mathbf{u}_e - \mathbf{u}_e^T \mathbf{K}_e^m \mathbf{u}_e \quad (1.10)$$

As a special case, if the element is deleted, i.e., replaced with void, we have an increase in compliance given by:

$$\Delta J_e^{k \rightarrow \emptyset} = \mathbf{u}_e^T \mathbf{K}_e^k \mathbf{u}_e \quad (1.11)$$

Similarly, as a special case of Equation 1.10, if a new element is inserted (in place of a void), we have a decrease in compliance by:

$$\Delta J_e^{0 \rightarrow m} = -\mathbf{u}_e^T \mathbf{K}_e^m \mathbf{u}_e \quad (1.12)$$

The element sensitivity in Equation 1.10 can be generalized to other quantities of interest. Specifically, for any quantity of interest  $Q$ , the first-order sensitivity is given by:

$$\Delta J_e^{k \rightarrow m} = -\boldsymbol{\lambda}_e^T \mathbf{K}_e^k \mathbf{u}_e + \boldsymbol{\lambda}_e^T \mathbf{K}_e^m \mathbf{u}_e \quad (1.13)$$

where  $\boldsymbol{\lambda}$  is the adjoint field associated with the quantity of interest. Thus, there is no fundamental restriction of the proposed method to compliance problems. The specific expression for the adjoint depends on the quantity of interest; for example, for the p-norm stress, an expression for the adjoint is derived in [18].

Similarly, the change in mass is given by:

$$\Delta M_e^{k \rightarrow m} = \rho^m V_e - \rho^k V_e \quad (1.14)$$

where  $\rho$  denotes (real) material density and  $V_e$  denotes volume of an element. Given this background, we now consider the two sub-steps to generate Pareto-optimal multi-material designs.

### Reducing Mass

Consider the mass-compliance plot of Figure 1.5. In this sub-step, our objective is to reduce mass, i.e., we swap materials only if  $\Delta M_e^{k \rightarrow m} < 0$ . Thus, only quadrants 2 and 3 in Figure 1.5 are acceptable. Further, quadrant 3 is preferable, since both mass and compliance are reduced.

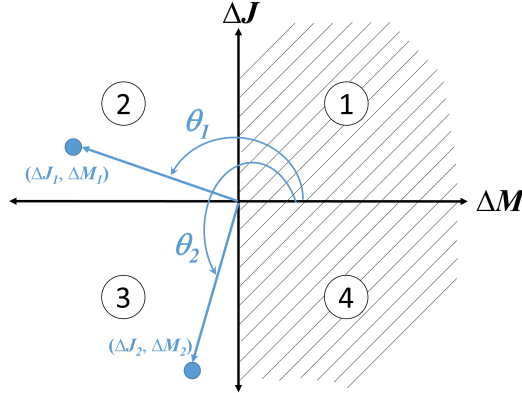


FIGURE 1.5: Reducing mass.

Thus, for each element, we must find a suitable material  $m$  such that the angle  $\theta$  is maximized, or equivalently,

$$\begin{aligned} & \underset{m}{\text{minimize}} -\theta_e^{k \rightarrow m} \equiv \frac{-\Delta J_e^{k \rightarrow m}}{\Delta M_e^{k \rightarrow m}} \\ & \text{subject to} \\ & \Delta M_e^{k \rightarrow m} < 0 \end{aligned} \quad (1.15)$$

Thus, in the first sub-step, for each element, we must find the material  $m$  that gives the lowest value of  $-\theta_e^{k \rightarrow m}$ . As a first step, we perform a finite element analysis and compute the compliance sensitivity for each element, as given by Equation 1.5. Next, for *each element* we compute the sub-step 1 ranking parameter:

$$r^1(e) = \min_m \left\{ \frac{-\Delta J_e^{k \rightarrow m}}{\Delta M_e^{k \rightarrow m}} \mid \Delta M_e^{k \rightarrow m} < 0 \right\} \quad (1.16)$$

The array  $r^1$  is sorted in an increasing order. After sorting, the first element in this list will be the best candidate to consider for material swapping, and so on. The number of elements to swap in this sub-step is chosen so as to result in a desired reduction in mass of  $\Delta M$ . Thus, we traverse down the sorted list of elements, and execute the swapping, until the desired reduction in mass is reached.

### Reducing Compliance

In this sub-step, our objective is to reduce compliance, i.e., we swap the material associated with an element, only if  $\Delta J_e^{k \rightarrow m} < 0$ . Thus, only quadrants 3 and 4 in Figure 1.6 are acceptable. Further, the compliance is minimized if the angle is close to  $\frac{3\pi}{2}$ .

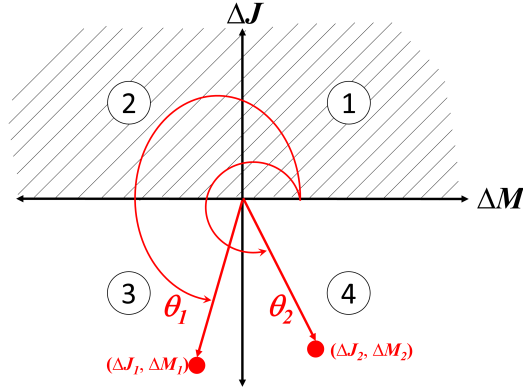


FIGURE 1.6: Reducing compliance.

Thus, for each element, we solve the following minimization problem (a linear search among all materials):

$$\begin{aligned} & \underset{m}{\text{minimize}} \left| \theta_e^{k \rightarrow m} - \frac{3\pi}{2} \right| \equiv \text{sign}(\Delta M_e^{k \rightarrow m}) \frac{\Delta J_e^{k \rightarrow m}}{\Delta M_e^{k \rightarrow m}} \\ & \text{subject to} \\ & \Delta J_e^{k \rightarrow m} < 0 \end{aligned} \quad (1.17)$$

As in the previous sub-step, we perform a finite element analysis, and compute the compliance sensitivity for each element, as given by Equation 1.5. Next, for *each element* we compute the sub-step 2 ranking parameter:

$$r^2(e) = \min_m \left\{ \text{sign}(\Delta M_e^{k \rightarrow m}) \frac{\Delta J_e^{k \rightarrow m}}{\Delta M_e^{k \rightarrow m}} \mid \Delta J_e^{k \rightarrow m} < 0 \right\} \quad (1.18)$$

The array  $r^2$  is sorted in an increasing order. The first element in the sorted list will be the best candidate to consider for material swapping, and so on. The number of elements to swap in this sub-step

should result in a desired reduction in mass of  $\Delta M$ . Therefore, we traverse down the sorted list of elements, until the desired reduction is reached.

Sub-steps 1 and 2 are repeated (see Figure 1.4) until there is no further improvement in compliance. We have observed in our numerical experiments that, typically, three-to-four iterations of the two sub-steps are sufficient to converge to the local Pareto-optimal design.

---

## 1.4 Numerical Experiments

In this section, we demonstrate the validity of the proposed method through several 3D examples. The material properties used in these experiments are summarized in Table 1.1;  $E$ ,  $\nu$ , and  $\rho$  denote Young's modulus, Poisson ratio, and density, respectively. In all examples, a uniform voxel mesh is used to discretize the domain.

Table 1.1: Material Properties.

Material	$E(\text{GPa})$	$\nu$	$\rho(\text{Kg/m}^3)$
A	105	0.3	5400
B	70	0.3	2700
C	140	0.3	8100
Copper-PLA (40%-60%)	45.2	0.33	4340
Aluminum-PLA (40%-60%)	28.8	0.33	1836

### 1.4.1 L-Bracket: Single and Two-Material Design

First, we consider the L-bracket illustrated in Figure 1.7a; all dimensions are in meters. The geometry is fixed at the top and a force of 100,000 N is applied at the center as illustrated in Figure 1.7b. This is a 3D version of a similar 2D problem posed in [6].

Given this structural problem, we consider: (1) a single material A, and (2) two materials A and B. The geometry is discretized using 50,000 hexahedral elements are used for both experiments. The objective is to minimize compliance, and to maintain consistency, the mass is reduced by 70% reduction in both cases. As stated earlier in the algorithm, we start with the heaviest design (all A) and optimize the topology and material distribution. The final optimized designs for the two cases are illustrated in Figure 1.8a and Figure 1.8b respectively. Note that the smooth material plot in Figure 1.8b is an artifact of vertex shading, whereas, in reality, the material assignment is element-wise discrete.

After the optimization process is complete, we obtain the two Pareto curves illustrated in Figure 1.9. As expected, for a given weight fraction, the two-material design is less compliant (stiffer) than the corresponding single material design.

Figure 1.10 illustrates the number of pre-conditioned CG iterations for single material TO, and dual-material TO. As one can observe, the single-material TO took about 200 FEA operations to complete, while the multi-material TO took about 180 FEA operations to complete. Further, the

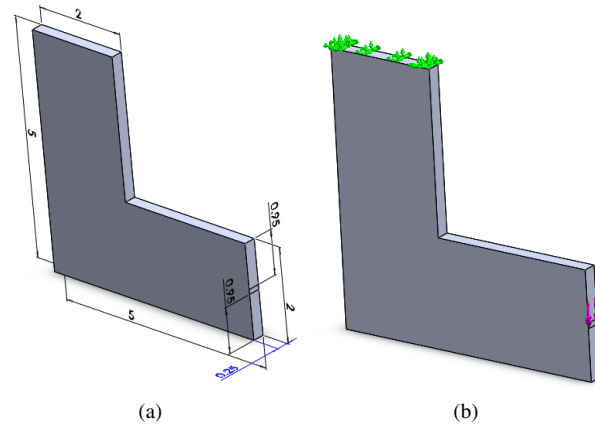


FIGURE 1.7: L-bracket: (a) dimensions, and (b) structural problem.

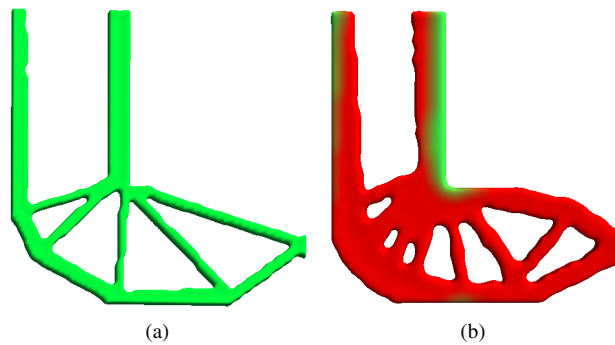


FIGURE 1.8: Optimized L-bracket at 0.30 mass fraction using (a) only material A and (b) both materials A and B.

CG iterations are moderately higher for multi-material TO. Overall, for this example, the cost of multi-material design is almost identical to the cost of single-material design.

### 1.4.2 Cantilever Beam

In this experiment, we consider three materials A, B, and C. The material properties are summarized in Table 1.1. The geometry and boundary conditions are illustrated in Figure 1.11. The design is discretized using 50,000 elements, i.e. 159,300 degrees of freedom. Beginning with all C initial design (heaviest and stiffest), the objective is to reduce mass by 80% while keeping the design as stiff as possible. Figure 1.11 illustrates the designs produced through optimization process while tracing the Pareto frontier.

Figure 1.12 illustrates 3 optimized designs with similar mass, but with different choices for the number of materials. Observe that as more materials are considered, the performance consistently improves (in the figure,  $J_0$  is the initial compliance, that is identical for all three designs)

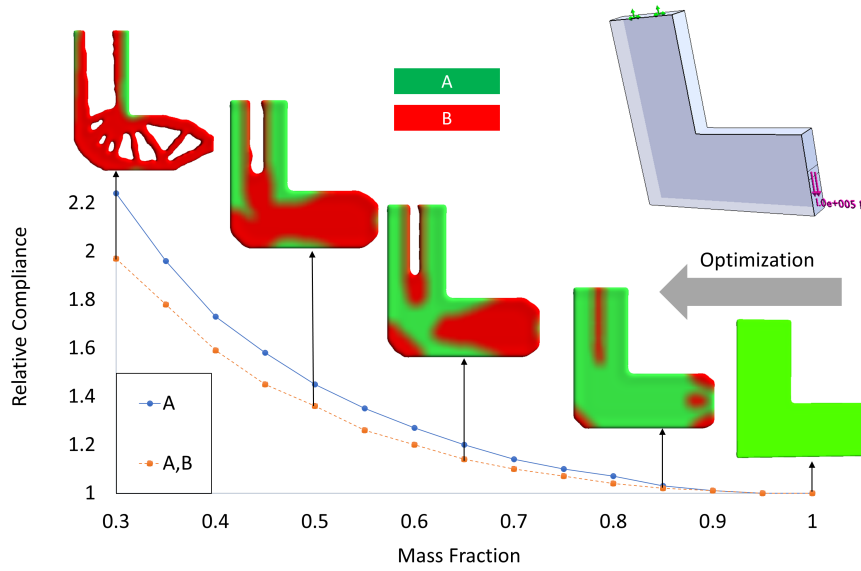


FIGURE 1.9: The Pareto curves for single material (A) and two materials (A and B).

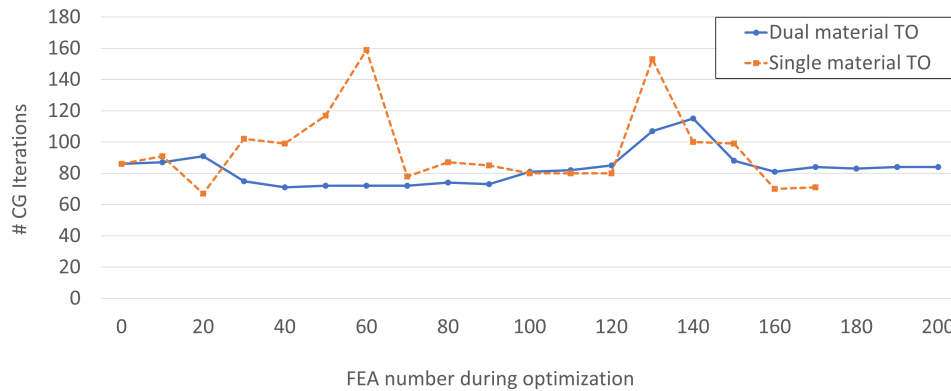


FIGURE 1.10: CG iterations for the L-Bracket with (a) single material A, (b) two materials A and B.

### 1.4.3 Mount-Bracket

This example focuses on demonstrating robustness and efficiency of the proposed method via a more complex design. Consider the mount bracket of Figure 1.13a, and its corresponding boundary conditions. The domain is discretized into 100,000 hexahedral elements with 378,732 degrees of freedom.

In this example, we consider Copper-PLA and Aluminum-PLA filaments with properties summarized in Table 1.1. The copper filament matrix is both stiffer and heavier. Given these material choices, starting with the stiffest and heaviest initial design, the objective is to reduce mass by 60%. Using both materials (1.13c) reduces compliance of final design by about 13%, relative to the single material design (1.13b).

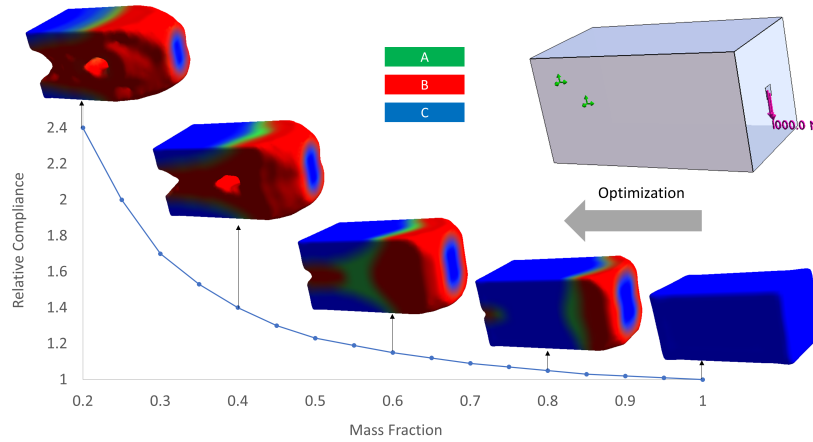


FIGURE 1.11: Optimized cantilever beam at 0.2 mass fraction with materials A, B, and C.

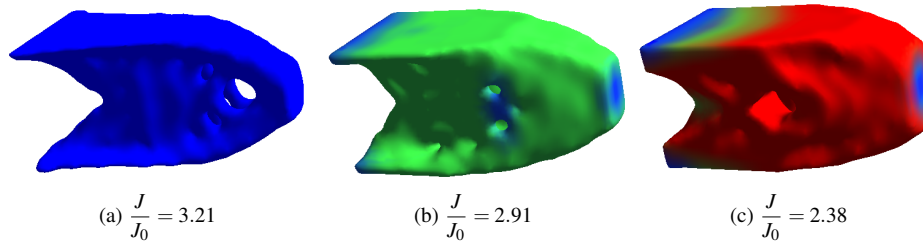


FIGURE 1.12: Optimized cantilever beam at 0.20 mass fraction using (a) only material C, (b) materials A and C, and (c) materials A, B, and C.

### Robustness of Pareto Tracing

To illustrate the robustness of the Pareto-tracing algorithm for the two-material distribution, we generated a random initial material distribution, of 0.7 mass fraction. Thus, we first need to find the corresponding Pareto-optimal design of 0.7 mass fraction through the algorithm of Figure 1.4. As illustrated in Figure 1.14, the algorithm was able to successfully find the Pareto-optimal design, and is consistent with the design found earlier at the same mass fraction. Further, the Pareto-tracing algorithm can continue to find other Pareto-optimal designs as illustrated in Figure 1.14.

### Run times and Memory Requirements

For all the experiments presented in this section, Table 1.2 summarizes the degrees of freedom, the target weight (or cost), total run-time, and required memory. All experiments were conducted on an Intel Core i7 CPU running at 3.4 GHz with 8GB of memory. Observe that all of the optimizations are completed in a matter of minutes, and use the limited memory (in the order of a tens of Mega-Bytes).

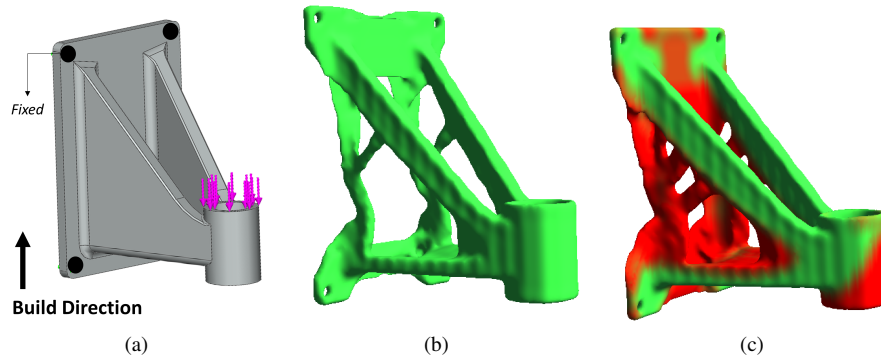


FIGURE 1.13: (a) Mount bracket, geometry and boundary conditions (b) optimized design at mass fraction of 0.4 using only A and (c) A and B.

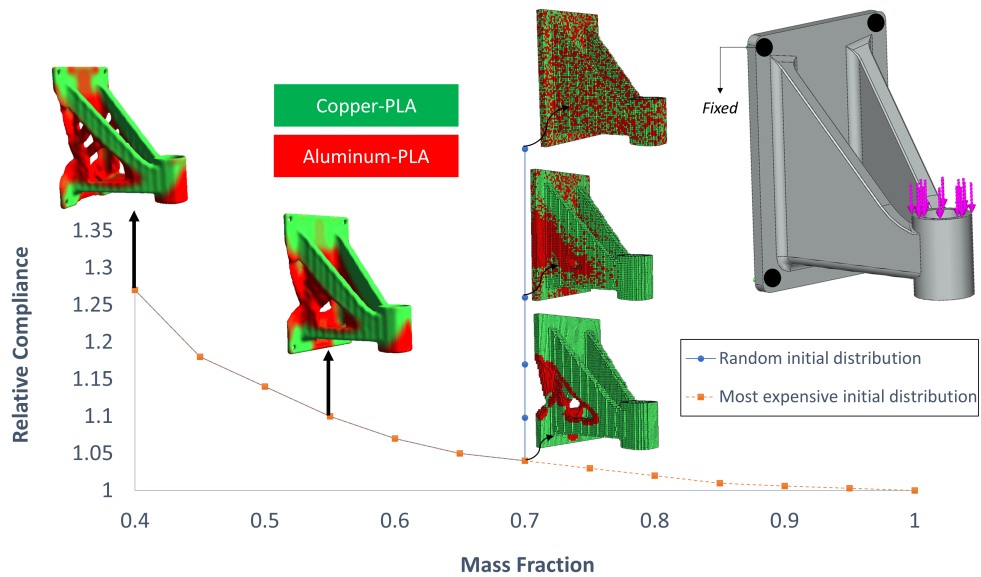


FIGURE 1.14: Mount bracket with random initial material distribution.

## 1.5 Contributions

In this chapter, we have made the following technical contributions:

1. Present a generalized multi-material topology optimization formulation for various cost functionals such as mass or price.
2. Discuss the multi-material sensitivity analysis.
3. Propose an efficient multi-material topology optimization algorithm based on Pareto tracing.

Table 1.2: Summary of computational costs.

Example	#DOF	Target weight	Time
L-bracket	168,750	30%	10 min.
Beam	159,300	20%	8 min
Mount Bracket	378,732	40%	20 min

4. Demonstrate the effectiveness of this scheme through numerical experiments.

This work can be viewed as an extension of the work presented in [17, 8]. The mesh independency of the single-material Pareto method is discussed in [18]; its extension to multi-material needs to be investigated.

---

## 1.6 Acknowledgements

The authors would like to thank the support of National Science Foundation through grants CMMI-1561899, IIP-1500205, through grants CMMI-1232508, CMMI-1161474, and DOE through ARPA-E ARID grant. Prof. Krishnan Suresh is a consulting scientific officer for SciArt, C-Corp, which has licensed the Pareto technology reported in this publication, through Wisconsin Alumni Research Foundation.

---

**References**

- [1] Grgoire Allaire, Charles Dapogny, Gabriel Delgado, and Georgios Michailidis. Multi-Phase Structural optimization Via A Level-set Method. *Control Optimisation and Calculus of Variations*, pages 576–611, 2014.
- [2] Jos Pedro Blasques. Multi-material topology optimization of laminated composite beams with eigenfrequency constraints. *Composite Structures*, 111:45–55, May 2014.
- [3] Luciano Pereira Chaves and Jesiel Cunha. Design of carbon fiber reinforcement of concrete slabs using topology optimization. *Construction and Building Materials*, 73:688–698, December 2014.
- [4] Niek de Kruijf, Shiwei Zhou, Qing Li, and Yiu-Wing Mai. Topological design of structures and composite materials with multiobjectives. *International Journal of Solids and Structures*, 44(2223):7092–7109, November 2007.
- [5] R. A. Feijoo, A. A. Novotny, E. Taroco, and C. Padra. The topological-shape sensitivity method in two-dimensional linear elasticity topology design. *Applications of Computational Mechanics in Structures and Fluids*, 2005.
- [6] Tong Gao and Weihong Zhang. A mass constraint formulation for structural topology optimization with multiphase materials. *International Journal for Numerical Methods in Engineering*, 88(8):774–796, November 2011.
- [7] Seung Hyun Jeong, Dong-Hoon Choi, and Gil Ho Yoon. Separable stress interpolation scheme for stress-based topology optimization with multiple homogenous materials. *Finite Elements in Analysis and Design*, 82:16–31, May 2014.
- [8] Amir M. Mirzendehtdel and Krishnan Suresh. A Pareto-Optimal Approach to Multimaterial Topology Optimization. *Journal of Mechanical Design*, 137(10):101701–101701, August 2015.
- [9] Amir M. Mirzendehtdel and Krishnan Suresh. Support structure constrained topology optimization for additive manufacturing. *Computer-Aided Design*, 81:1–13, December 2016.
- [10] A. A. Novotny, R. A. Feijo, E. Taroco, and C. Padra. Topological sensitivity analysis for three-dimensional linear elasticity problem. *Computer Methods in Applied Mechanics and Engineering*, 196(41):4354–4364, 2007.
- [11] Jaejong Park and Alok Sutradhar. A multi-resolution method for 3d multi-material topology optimization. *Computer Methods in Applied Mechanics and Engineering*, November 2014.
- [12] Anand Ramani. A pseudo-sensitivity based discrete-variable approach to structural topology optimization with multiple materials. *Structural and Multidisciplinary Optimization*, 41(6):913–934, June 2010.
- [13] Anand Ramani. Multi-material Topology Optimization with Strength Constraints. *Struct. Multidiscip. Optim.*, 43(5):597–615, May 2011.
- [14] O. Sigmund. Design of multiphysics actuators using topology optimization Part II: Two-material structures. *Computer Methods in Applied Mechanics and Engineering*, 190(4950):6605–6627, October 2001.
- [15] Ole Sigmund and Kurt Maute. Topology optimization approaches. *Structural and Multidisciplinary Optimization*, 48(6):1031–1055, December 2013.

- [16] Krishnan Suresh. Efficient generation of large-scale pareto-optimal topologies. *Structural and Multidisciplinary Optimization*, 47(1):49–61, May 2012.
- [17] Krishnan Suresh. Topology Optimization on the Cloud: A Confluence of Technologies. In *ASME 2015 International Design Engineering Technical Conferences and Computers and Information in Engineering Conference*, pages V01AT02A041–V01AT02A041. American Society of Mechanical Engineers, 2015.
- [18] Krishnan Suresh and Meisam Takaloozadeh. Stress-constrained topology optimization: a topological level-set approach. *Structural and Multidisciplinary Optimization*, 48(2):295–309, March 2013.
- [19] J. Thomsen. Topology optimization of structures composed of one or two materials. *Structural optimization*, 5(1-2):108–115, March 1992.
- [20] Natasha Vermaak, Georgios Michailidis, Guillaume Parry, Rafael Estevez, Grgoire Allaire, and Yves Brchet. Material interface effects on the topology optimization of multi-phase structures using a level set method. *Structural and Multidisciplinary Optimization*, pages 1–22, June 2014.
- [21] Michael Yu Wang, Shikui Chen, Xiaoming Wang, and Yulin Mei. Design of Multimaterial Compliant Mechanisms Using Level-Set Methods. *Journal of Mechanical Design*, 127(5):941–956, January 2005.
- [22] Michael Yu Wang and Xiaoming Wang. Color level sets: a multi-phase method for structural topology optimization with multiple materials. *Computer Methods in Applied Mechanics and Engineering*, 193(6-8):469–496, February 2004.
- [23] Xiaoming Wang, Yulin Mei, and Michael Yu Wang. Level-set method for design of multi-phase elastic and thermoelastic materials. *International Journal of Mechanics and Materials in Design*, 1(3):213–239, September 2004.
- [24] Yiqiang Wang, Zhen Luo, Zhan Kang, and Nong Zhang. A multi-material level set-based topology and shape optimization method. *Computer Methods in Applied Mechanics and Engineering*, 283:1570–1586, January 2015.
- [25] L. Yin and G. K. Ananthasuresh. Topology optimization of compliant mechanisms with multiple materials using a peak function material interpolation scheme. *Structural and Multidisciplinary Optimization*, 23(1):49–62, December 2001.